FTS option for SPEC-BOL
Swinging triangle Fourier transform spectrometer
(SWIFT)

Kjetil Dohlen

dohlen@obmara.cnrs-mrs-fr

Laboratoire d'Optique, Observatoire de Marseille
2 Place Le Verrier, 13248 Marseille Cedex 4, France

1. Introduction

A Fourier transform spectrometer (FTS) for the spectrometer channel of the FIRST bolometer instrument is presented. Based upon the Martin-Puplett polarizing interferometer, it is original in using a rotational displacement mechanism.

In the following we present preliminary analysis of the theory of operation and the optical layout allowing its integration within the instrument space envelope.

2. First-order parameters

Scientific specifications for the BOL spectrometer channel demands a resolving power of 1000 at 250 μm and diffraction-limited imaging over a field of view of 2 x 2 arcminutes. It has been found that this performance is best met by Fourier transform spectroscopy (FTS). A Martin-Puplett-type instrument producing single-sided interferograms is considered optimal for the given waveband.

2.1. Optical path length

For single-sided interferograms, required variation in optical path length is directly related to nominal resolving power by:

$$\mathrm{OPD} = R\ \ l/\,2 \tag{1}$$

For R = 1000 and λ=250 μm, the required optical path difference is OPD = 125 mm. Required physical scan length varies between 1/2 and 1/8 of this according to the scanning scheme implemented.

2.2. Beam diameter

Minimizing the diameter of the collimated beam within the interferometer is important in order to minimize the size of the instrument and its optical components. We discuss the limiting factors.

2.2.1. The spectral spread problem

For a beam diameter of *d* within the instrument and a telescope aperture diameter of *D*, the FOV on the sky translates into an internal beam angle of:

$$b = \frac{\mathrm{FOV}\ D}{2d} \tag{2}$$

A beam passing through the interferometer at an angle to the axis does not see the same optical path difference as an axial beam. The actual OPD for a beam at angle *b* is given by:

$$\mathrm{OPD}' = \mathrm{OPD}\cos b \tag{3}$$

where OPD is measured along the axis. The apparent wavenumber (s') of the incident radiation is proportional to the rate of change of the OPD, hence:

$$s' = s\cos b\ , \tag{6}$$

where s is the wavenumber as measured for an axial beam.

For an imaging FTS, the average angular position is different for each pixel. The wavenumber scale must therefore be recalculated for each pixel. Also, since each pixel covers a certain angular range, there is an uncertainty in the wavenumber measured by a pixel since the apparent wavenumber varies from one edge of the pixel to the other. This spread limits the resolving power of the instrument.

Differentiating eq. 6 gives:

$$ds = -s \sin b \; db \approx -s \; b \; db \tag{7}$$

for small angles. Hence the resolving power for a pixel of angular width Δb is limited to:

$$R < s / \Delta s = 1/(b \; \Delta b) \tag{8}$$

Assuming diffraction limited imaging with critical sampling at the shortest wavelength, the angular pixel size is:

$$\Delta b = l_{\min} /(2d) \tag{9}$$

Substituting equations 2 and 9 into eq. 8 we get::

$$R < \frac{4d^2}{l_{\min} D \; \mathrm{FOV}} \tag{10}$$

Hence, reorganizing:

$$d > \frac{\sqrt{R \, l_{\min} D \; \mathrm{FOV}}}{2} \tag{11}$$

For D = 3280 mm, FOV = 2 arcmin = 0.58 mrad, λ_{min} = 200 μm and R > 1000, we need d > 9.8 mm.

2.2.2. The wavefront shear problem

An other problem which must be taken into account for an imaging FTS is that of wavefront shear. The two recombining wavefronts are displaced laterally by a distance

$$\Delta d = \mathrm{OPD} \sin b \approx \mathrm{OPD} \; b \tag{12}$$

Dividing both sides by d and substituting eq. 2, the relative wavefront shear is:

$$c = \frac{\Delta d}{d} = \frac{\mathrm{OPD} b}{d} = \frac{\mathrm{OPD} \; D \; \mathrm{FOV}}{4d^2} \tag{12}$$

Reorganizing:

$$d = \sqrt{\frac{\mathrm{OPD} \; D \; \mathrm{FOV}}{4 \, c}} \tag{13}$$

Wavefront shear reduces interferogram quality in two ways:

- **Overlap area**

Only the overlapping area of the wavefronts actually interfere, the edges which do not overlap only add to the background signal, hence lowers the interferogram contrast. This may be encountered by using an undersized pupil stop after the interferometer, but only at some loss of energy for all pixels. Assuming no such undersizing, the contrast reduction due to this effect is seen to be equal to the ratio of the area of overlap to the total pupil area. By analogy to the calculation of MTF for a perfect lens, the contrast assuming a circular pupil may be given by [2]:

$$k_O = (2/p)\left(\cos^{-1} c - c\sqrt{1-c^2} \right). \tag{14}$$

- **Coherence**

The part of the wavefront which actually interferes sees a contrast reduction due to the limited spatial coherence of the wavefront emanating from an extended source. This is governed by the van Cittert-Zernike theorem [3] which may be stated as:

$$k_C = 2J_1(u)/u \tag{15}$$

where J_1 is the Bessel J function of the 1st order, $u = (2p/l)\Delta d\, r/f$, r is the radius of the source, and f is the source distance. The effective source area seen by each detector equals that of the detector projected onto the source. We may therefore define r as the detector radius and f as the camera focal length. Then, since Δb is the angular diameter of a pixel and applying eq. 9:

$$r/f = \Delta b/2 = l_{\min}/(4d)\,. \tag{16}$$

The argument of the Bessel function then becomes:

$$u = \frac{p}{2}\frac{l_{\min}}{l}\frac{\Delta d}{d} = \frac{p}{2}\frac{l_{\min}}{l}\,c\,. \tag{17}$$

Figure 1 plots these two effects versus fractional shear. Clearly, the dominant effect is that due to overlap area. For a contrast superior to about 90%, the shear should not exceed 0.1. For OPD = 125 mm, D = 3280, FOV = 2 arcmin = 0.58 mrad, eq. 13 therefore demands a beam diameter greater than 24 mm.

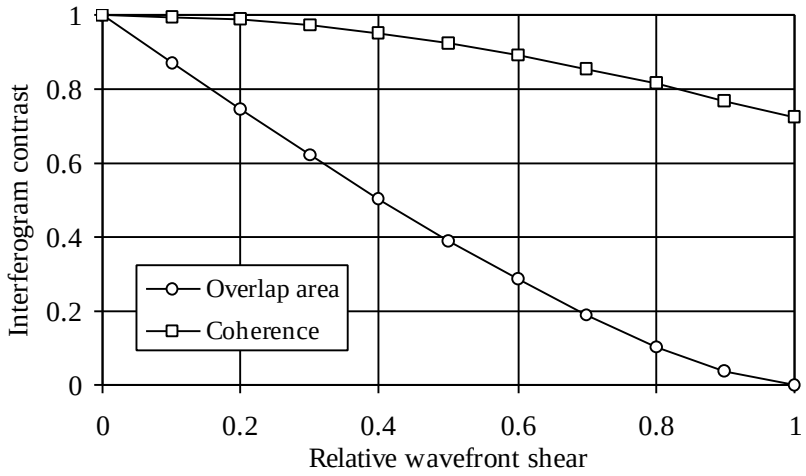

Figure 1. The effects of wavefront shear upon interferogram contrast. The coherence effect is calculated for $l_{min}/l = 1$.

2.2.3. Beam diameter, conclusion

Contrast reduction due to wavefront shear is seen to be the most constraining parameter for beam diameter determination. A contrast reduction not exceeding 10% at the edge of the FOV and at maximum optical path difference demands a beam size greater than 24 mm. We have chosen a beam size of d = 30 mm so as to leave some margin.

3. Interferometer concept

The Martin-Puplett interferometer [1] consists of an input polarizer (P1), a beam splitting polarizer (BS), two roof-top mirrors (RT1, RT2), an output polarizer (P2) and two detectors (D1, D2). In addition to the source to be studied (S) a black-body reference source (BB) is required.

P1 is mounted at an angle to the incoming beam, reflecting one polarization component out of the optical path while transmitting the other into the interferometer. It also serves to inject the reference beam from the BB into the instrument, the BB being mounted such that it is seen from the instrument through a reflection in P1. The science beam and the reference beam thus exists simultaneously in the instrument at opposite polarizations. The polarizing axis of the BS is oriented at 45° to that of P1, thus splitting each beam into two equal, linearly polarized components, one transmitted, the other reflected.

The roof top mirrors introduce two metallic reflections. Assuming perfectly conducting surfaces, one reflection introduces a 45° phase shift between the parallel and perpendicular polarization components regardless of polarization state and angle of incidence of the incoming ray. A linearly polarized beam therefore becomes circularly polarized. The second reflection restores linear polarization but the direction of polarization is rotated by 90°.

Back at the BS the beam previously reflected now gets transmitted and vice versa. The BS thus has 100% efficiency; all the incident radiation is transmitted towards the detectors. Four component beams are superposed: two orthogonal polarizations from the BB and two from the source. Each component beam contains the interferometric information, but the information is of opposite sign in each of the orthogonal polarizations; the total is hence equal to zero. The interferometric information is restored by the second polarizer (P2) oriented in the same direction as P1. Orthogonal components are then separated, one reflected onto detector D1 and the other transmitted onto D2.

Since the action of P1 was to transmit to the interferometer opposite polarizations of BB and S, the interferometric information transmitted to each detector has opposite sign for BB and S. Therefore both of the detected interferograms represents the difference between the spectra of the two sources. This has the advantage of greatly reducing (even eliminating) the central maximum of the interferogram, thus limiting the dynamic range required for detection and telemetry.

3.1. The swinging triangle concept

In addition to its polarizing properties, the roof top mirror has the advantage of being insensitive to a rotation around the line of intersection (vertex) of the mirrors: neither the optical path undergone nor the displacement of a ray entering the system is affected by such a rotation, however big (as long as the mirrors themselves are big enough). A translation perpendicular to the intersection line does not affect optical path difference but it does displace the output beam with respect to the input beam. The change in ray displacement is twice the roof top displacement.

3.1.1. Ideal operation

In the swinging triangle Fourier transform spectrometer (SWIFT) concept, the RTs are mounted on two arms of length l rotating about a common axis. At zero OPD the arms are perpendicular to the incoming beam. A rotation of the arms through an angle Δf thus translates into a longitudinal translation of the roof-top vertices of $z = l \sin\Delta f$ and a transverse translation of $y = l\,(1 - \cos\Delta f)$. The movement is identical for the two RTs. As we have seen above, the transverse displacement simply displaces the output beam with respect to the input beam.

The longitudinal translation introduces an optical path difference between the recombined beams of OPD = 4 z, a factor 2 due to the double passage and another factor 2 since the two mirrors move simultaneously. For a resolving power of $R = 1000$ at $l = 250$ μm and assuming single-sided interferograms, we require OPD = $R\ l/2 = 125$ mm, hence $z = \text{OPD}/4 = 31.25$ mm. With arms of length $l = 150$ mm, the angular movement must therefore be $\Delta f = \text{asin}(z/l) = 12.0°$. Under these conditions the transverse movement of the RT is 3.3 mm. Arranging the input beam such as to be centred on the RTs for an appropriate angular position, the "walk" of the output beam may be arranged to be ±3.3 mm to either side of the nominal (incoming beam) position, i.e. 10% of the beam diameter for a 30 mm beam.

The beam walk must be taken into account when designing the optics, but it has no effect upon the instrument performance.

3.2. Perturbed operation

We may consider three different types of perturbations of the SWIFT:

- Rotation of the interferometer wrt the optical axis of the camera system
- Tilt of the BS
- Displacement of the rotation axis

Interferometer rotation modifies the angular position of each pixel, hence, according to eq. 6, the spectral calibration.

BS tilt and rotation axis displacement produce an apparent transverse movement of the roof-tops with respect to each other. While BS tilt is probably constant or very slowly varying, rotation axis displacement may be expected to vary during a scan due to asymmetries in the flexure pivots. A transverse movement which is strictly linear and zero at zero OPD is equivalent to a rotation of the interferometer and introduces therefore a change in calibration.

A constant or non-linear transverse movement modifies the spectral line function (SLF) in a more subtle manner. A computational model is required to establish the effects of such perturbations. Our experience from the IASI instrument (infrared atmospheric sounding interferometer) where an extremely detailed knowledge of the SLF was required, shows that off-axis pixels are particularly sensitive and that apodization very efficiently reduces the sensitivity. Although the present instrument probably requires less strict SLF knowledge specifications, a computer model should be constructed to evaluate the phenomenon and fix tolerance specifications.

The present note limits itself to perturbations of the spectral calibration. As seen in eq. 6, the apparent wavenumber of a spectral line varies with angular distance from the optical axis. Any variations in this angular distance thus introduces a spectral shift. Clearly, since each pixel has a different angular distance from the axis, the on-ground spectral calibration has to be done individually for each one. It is the deviations from this calibration which are considered.

3.2.1. Definition of axes

We consider two axes in our system which should be parallel under unperturbed operation, see Figure 2

The axis referred to as the *detector axis* has the direction of a collimated beam in the interferometer space which is focussed by the camera optics (Cam) onto the central point of the detector arrays.

The axis referred to as the *interferometer axis* has a direction which is perpendicular to the arm joining the rotation axis (A) and the roof-top vertex (C1) of the roof-top facing the output of the interferometer at the position of zero optical path difference.

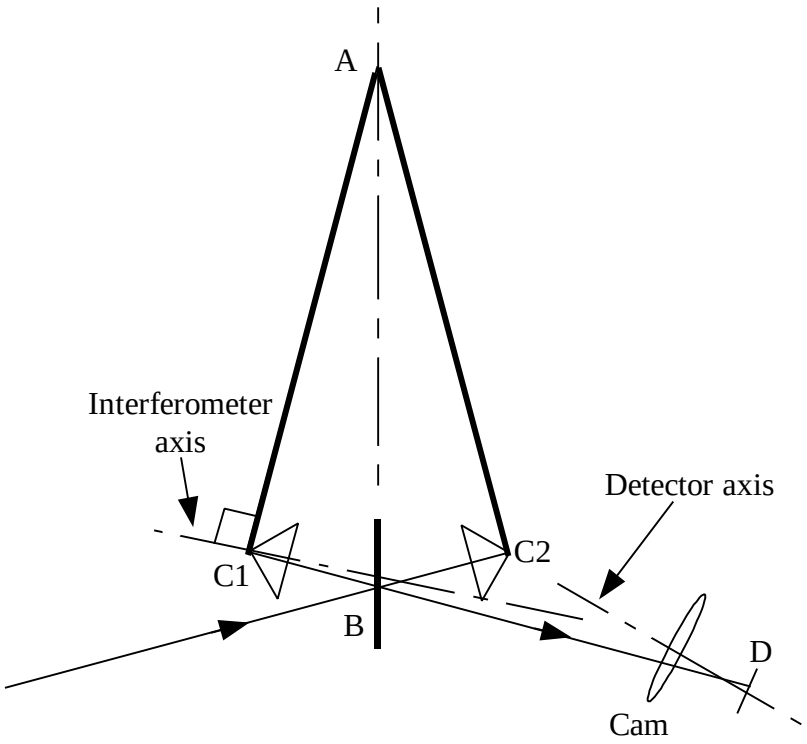

Figure 2 Definition of axes. A: nominal rotation axis, B: centre of beam splitter, C1, C2: roof-top vertex points, Cam: camera optics, D: detector arrays.

3.2.2. Preliminary error budget allocation

Differentiating eq. 6 gives:

$$\frac{ds}{db} = -s \sin b \approx -s\,b \tag{20}$$

for small angles. Using eq. 2 to calculate the internal beam angle, the angular alignment tolerance may be given by:

$$|db| = \frac{2d}{\mathrm{FOV}\ D}\frac{ds}{s}. \tag{21}$$

For D = 3280 mm, FOV = 2 arcmin = 0.58 mrad, d = 30 mm, and a calibration error of a tenth of a resolution element, ds/s = 1/(10 R) = 1/10 000 when R = 1000, the global alignment tolerance is 3 mrad or 10 arcmin.

To produce a preliminary error budget, one may assume about 10 independent perturbations contributing to the calibration error. Each source may be allocated $1/\sqrt{10} \approx 1/3$ of the total tolerance, i.e. 1 mrad. This is then the allowed misalignment of the interferometer axis and the detector axis due to a single perturbation. It corresponds to a shift of the detector array of 0.15 mm when the camera focal ratio is F/5.

3.2.3. Scan axis displacements

Consider Figure 3 for the effect of a displacement of the scan axis. C0 is the zero OPD position of the roof-top facing the detectors, C1 is its position at after a scan through angle Δf, C2 is the position of the other roof-top, and C2′ is its apparent position as seen by the detector through the BS. We define a set of co-ordinate axes (x,y ,z), x perpendicular to the plane of the movement (i.e. of the paper), y along the line AB (in the plane of the BS), and z perpendicular to the two former. Clearly, a displacement along x has no effect other than a possible clipping of the beam. Displacements along y gives a movement of the roof-tops relative to the incoming beam causing a displacement of the outgoing beam similar to the displacement seen during a scan (see Sec. 3.1.1). There is no relative movement of C1 and C2′ however.

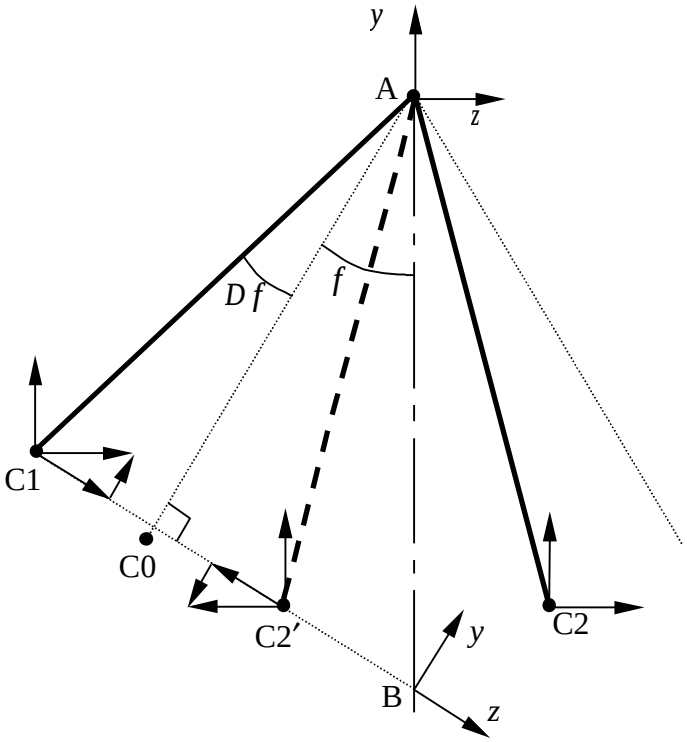

Figure 3. Illustration of the effect of scan axis displacements

Displacements along the z axis is less trivial, causing a movement of C1 and C2′ in opposite directions. Their movements may be decomposed in a co-ordinate system (x,y,z) where x is perpendicular to the paper, y is in the plane of the paper and perpendicular to the interferometer axis (Figure 2), and z is along the interferometer axis. A displacement Δz then produces the following relative movements of C1 and C2′:

$$\begin{aligned} \Delta x &= 0 \\ \Delta y &= 2\,\Delta z\ \sin f \\ \Delta z &= 2\,\Delta z\ \cos f \end{aligned} \tag{22}$$

where f is the angle C0 A B. Hence, such a displacement of the rotation axis provokes a modification of the OPD (Δz) and a lateral shift of the roof-top vertices (Δy).

A linear lateral shift corresponds to a tilt of the interferometer axis. At the maximum optical path difference where the separation between C1 and C2′ is OPD/4 = 31.25 mm, an acceptable tilt angle between the axes of 1 mrad corresponds to a lateral shift of about 0.03 mm. According to eq. 22, with $f = 30°$, the tolerance for an uncalibrated linear displacement of the scan axis is therefore 0.03 mm.

Table 1 summarizes the preliminary tolerances calculated for a spectral calibration accuracy of 1/10 spectral element.

Table 1. Summary of preliminary tolerances calculated for a spectral calibration accuracy of 1/10 spectral element.

Item	Tolerance
Rotation of interferometer axis wrt detector axis	1 mrad
Detector displacement	0.15 mm
Maximum excursion for a linear displacement of the scan axis	0.03 mm

4. Optical design

The proposed optical implementation of the SWIFT interferometer in the BOL space envelope consists of two separate systems, see Figure 4. The relay system (a) picks off the beam from the photometer optical train and feeds it into the spectrometer system (b). The spectrometer system provides a collimated beam of the right diameter for the interferometer and focuses the beam onto the detector arrays. The relay system provides a pupil image for the injection of the reference blackbody and for pupil clipping and baffling. The spectrometer system provides two pupil images, one at the interferometer and one just before the detectors for the location of a cold stop.

The optical design has yet to be “stitched together” so as to model the entire path including the FIRST telescope, photometer fore-optics, relay optics, and spectrometer optics. Note that it may be necessary to take the spectrometer into account when optimizing the photometer fore optics.

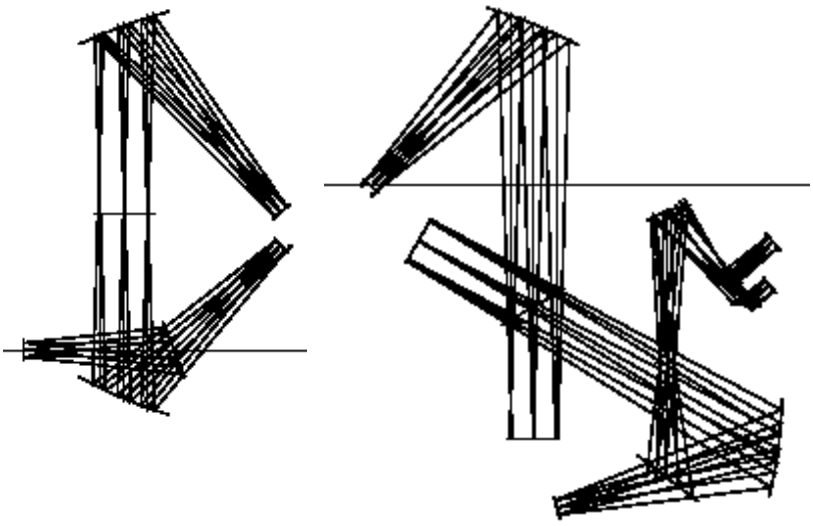

(a) (b)

Figure 4. Optical ray-trace of the two optical systems: relay system (a) and spectrometer system (b). The transparency of the flat folding mirrors is an artefact. The systems lie in two different planes, one perpendicular to the other. They are joined together with a toroidal Fabry mirror. The scale is ~1:5.

4.1. Relay system

The relay (Figure 4 a) consists of a toroidal Fabry mirror (PO) located in the intermediate image (F/4.5) following the chopper in the photometer optical train. The power of this mirror is calculated to correctly place

the pupil in the relay system and its toricity assures acceptable pupil image quality. Reflected off a flat folding mirror (R1), the beam is then collimated by an off-axis paraboloid (R2), sending the beam up in a light shaft between the two instruments towards another off-axis paraboloid (R3) refocusing the beam (F/5) into a focus (F). This combination of two off-axis paraboloids ensures virtually perfect imaging between the two focal planes. Half-way up the shaft is formed the pupil image in which a physical pupil mask may be placed. Just above this mask a polarizer is mounted at 45°, creating a second image of the pupil to one side of the shaft. The image is virtual as seen from the outside, but real as seen from the detector. Placing a blackbody reference source in this pupil plane ensures even reference irradiation of the detector arrays.

4.2. Spectrometer system

Another toroidal Fabry mirror in F redirects the beam into the spectrometer system (Figure 4 b). Again a couple of off-axis paraboloids constitute the main part of the optical system (Coll and Cam1). A second, toroidal, camera mirror (Cam2) is added to provide the cold stop pupil image. The optical quality of the spectrometer system is limited by the performance of this component, providing virtually perfect imaging at the centre of the FOV and a Strehl ratio of 0.95 in the corners of a 2′ by 2′ FOV. The image is flat.

The current model of the interferometer replaces the roof-top mirrors with plane mirrors, allowing raytracing at zero OPD. A more complete model requires considerable complications, notably introducing non-sequential raytracing.

5. Conclusions

The SWIFT spectrometer concept for the FIRST bolometer instrument is presented. A variation of the Martin-Puplett polarizing interferometer, its operation is described and preliminary tolerances to perturbations are estimated. Further work should include the construction of a computational model of the interferometer allowing more detailed tolerance calculations, notably of the spectral line function, and a more complete optical ray-tracing model.

6. References

[1] D. H. Martin and E. Puplett, Infrared Phys. **10**, 105 (1969)

[2] W. B. Wetherell, “The calculation of image quality”. In: *Applied Optics and Optical Engineering*, vol. VIII, ed.: R. Shannon and J. Wyant, Academic Press, London 1980.

[3] M. Born, E. Wolf, *Principles of Optics*, 6th edition, Pergamon Press, Oxford 1980.